International Journal of Coal Science & Technology (2023) 10:21
https://doi.org/10.1007/s40789-023-00576-7

RESEARCH

Effect of demineralization on pyrolysis characteristics of LPS coal based on its chemical structure

Lin Qian[1] · Jinkai Xue[1] · Chao Tao[1] · Chao Ma[2] · Xiaopeng Jiang[1] · Feiqiang Guo[1]

Received: 21 June 2022 / Revised: 11 September 2022 / Accepted: 1 March 2023

Abstract
The critical issue in developing mature Oxy-Coal Combustion Steam System technology could be the reactivity of demineralized coal which, is closely related to its chemical structure. The chemical structures of Liupanshui raw coal (LPS-R) and Liupanshui demineralized coal (LPS-D) were analyzed by FTIR and solid-state ^{13}C-NMR. The pyrolysis experiments were carried out by TG, and the pyrolysis kinetics was analyzed by three iso-conversional methods. FTIR and ^{13}C-NMR results suggested that the carbon structure of LPS coal was not altered greatly, while demineralization promoted the maturity of coal and the condensation degree of the aromatic ring, making the chemical structure of coal more stable. The oxygen-containing functional groups with low bond energy were reduced, and the ratio of aromatic carbon with high bond energy was increased, decreasing the pyrolysis reactivity. DTG curve-fitting results revealed that the thermal weight loss of LPS coal mainly came from the cleavage of aliphatic covalent bonds. By pyrolysis kinetics analysis of LPS-R and LPS-D, the apparent activation energies were 76 ± 4 to 463 ± 5 kJ/mol and 84 ± 2 to 758 ± 12 kJ/mol, respectively, under different conversion rates. The reactivity of the demineralized coal was inhibited to some extent, as the apparent activation energy of pyrolysis for LPS-D increased by acid treatment.

Keywords Demineralization · Chemical structure of coal · Coal pyrolysis · Pyrolysis kinetics · Iso-conversional

1 Introduction

As a major climate forcing factor, CO_2 mainly generated from fossil fuel combustion and coal-fired power stations are the largest source of CO_2 emissions (Cui et al. 2021; Leng et al. 2021; Liu et al. 2021). At present, controlling the emission of CO_2 is a key challenge for China to achieve the peak carbon in 2030. Oxy-fuel combustion technology, which can capture CO_2 from power plants, has become a hot topic in recent years (Zhang et al. 2021; Yang et al. 2021). Sun et al. (2012) proposed a system of Oxy-Coal Combustion Steam System (OCCSS) of near-zero emissions, which has high net power generation efficiency and near zero CO_2 emission. In OCCSS system, the fuel (ash-less coal) consumed by reacting with O_2 and steam in high pressure has to be pre-processed through demineralization. However, after demineralization treatment, the organic matter and chemical structure of demineralized coal will be altered to a certain extent, making the reactivity of which are quite different from that of the raw coal.

Pyrolysis is the first step in coal conversion and utilization, to what extent the pyrolysis proceeds depend on the chemical structure of the coal and the reaction conditions. Raman, FTIR, XRD, XPS etc. were commonly applied to investigate chemical structural characteristics of coal before and after acid treatment (Lin et al. 2017; Shi et al. 2013; Song et al. 2016; Ahmed et al. 2003; Li et al. 2019; Sonibare et al. 2010; Gómez-Serrano et al. 2003). Li et al. (2019) reported that the content of oxygen-containing functional groups in raw coal reduced through acid treatment by Raman. Lin et al. (2017) found that by HF-HCl combined acid treatment, the long aliphatic chain in coal was destroyed, the content of carboxyl group and phenolic hydroxyl group increased, the content of aliphatic and aromatic hydrogen decreased by FTIR. In order to study reactivity of coal before and after demineralization, a large number of pyrolysis experiments by thermogravimetric

✉ Lin Qian
5477@cumt.edu.cn

[1] School of Low-Carbon Energy and Power Engineering, China University of Mining and Technology, Xuzhou 221116, China

[2] State Key Laboratory of Clean Energy Utilization, Zhejiang University, 310027 Hangzhou, China

Published online: 18 April 2023

have been carried out (Slyusarskiy et al. 2017; Mandapati and Ghodke 2021). Cheng et al. (2020) found acid treatment did not dramatically alter the main devolatilization behavior of coals in a system that coupled DSC with a thermal gravimetric analyzer and a mass spectrometer. Zhu et al. (2019) reported that acid pretreatment increased the weight loss of lower rank coal with a thermogravimetric analysis. Liu et al. (2017a, b) found that acid treatment increased the pyrolysis reactivity of demineralized coal by both TGA and fixed bed experiments. However, Song et al. (2020) found that the pyrolysis reactivity of demineralized coal decreased on the contrary. In addition, some studies (Song et al. 2016; Cheng et al. 2019) indicated that the existence of minerals in ash is the main reason for the high reactivity of coal without demineralization, while the transformation and effect of inherent minerals in coal are relatively complex and still controversial (Li et al. 2017). Liu (2004) investigated that inherent minerals in coal did not have significant effect on the pyrolysis characteristics of coal. Qiu et al. (2014) found that the presence of alkaline earth metals reduced the pyrolysis reactivity of raw coal instead.

Based on previous studies, this paper focuses on the chemical structure of LPS-R and LPS-D (especially the functional groups and carbon structure), their pyrolysis characteristics and kinetic mechanism of pyrolysis, intended to describe the association between them, to better understand the effect of demineralization on coal pyrolysis reactivity. The influence of acid treatment on functional groups and carbon structure of LPS coal was discussed in this paper by FTIR and ^{13}C-NMR. Thermogravimetric analysis was used to study the pyrolysis of coal before and after demineralization at three heating rates of 20, 40 and 60 °C/min, respectively. To evaluate the role of acid treatment on coals' structure and reactivity, the pyrolysis kinetics was analyzed by iso-conversional methods like Starink, FWO and DAEM.

2 Material and methods

2.1 Samples preparation

LPS-D was obtained from LPS-R through HCl-HF-HCl three-stage acid treatment. The detailed description of specific acid treatment procedure was given elsewhere (Zhao et al. 2018). Both LPS-R and LPS-D pulverized, grounded and sieved to a particle size smaller than 75 μm were dried in a thermostat at 105 °C for 6 h. Table 1 showed the proximate and ultimate analysis of LPS-R and LPS-D, from which it can be seen that the ash content (dry basis) was significantly reduced from 15.62% (LPS-R) to 2.46% (LPS-D) after acid treatment. The mass fractions of H, N, and S (dry ash free basis) were nearly unchanged and the mass fraction of C (dry ash free basis) increased greatly after acid pretreatment.

2.2 FTIR and solid-state ^{13}C-NMR

The functional groups in samples were characterized by a German Bruker VERTEX 80 V Fourier transform infrared spectrometer, with a scanning range of 350–4000 cm^{-1} and a scanning number of 32. In sample preparation, firstly taking 2 mg pulverized coal and KBr to mix at a mass ratio of 1:100, and then grinding the mixed sample to powder form.

The solid-state ^{13}C-NMR detection were performed by AVANCE III-600 MHz NMR fully digital superconducting NMR instrument from Bruker, Germany. The experiment was performed by using a 4 mm MAS probe with a magic angle rotation of 14 kHz and a resonant frequency of 150.9 MHz. The cross-polarization contact time was 2 ms and the cycle delay time was 6 s.

Peak Fit version 4.12 software was used to divide the absorption peaks obtained by both FTIR and ^{13}C-NMR. By analyzing the second derivative of spectral data, the approximation of the position and number of fitting peaks was obtained. The residual sum of squares between the original spectrum and the fitting spectrum was considered as the minimum objective function for fitting, and the fitting spectrum was continuously optimized by adjusting the parameters of the fitting peaks.

2.3 TGA experiments

Pyrolysis of the coals was conducted on a TGA/SDTA851e thermogravimetric analyzer. The pyrolysis process was carried out in 99.999% high purity Ar atmosphere with a flow rate of 80 mL/min. The coal samples were heated from 25 °C to 1000 °C at 20, 40 and 60 °C/min, respectively, and the weight of the coals used in each experiment was about 26 mg. When 1000 °C is reached, a cooling ramp was initiated at 20 °C/min in the program to restore the system to room temperature. A group of empty crucible control experiments were carried out in each group of working conditions. Do at least two parallel experiments.

Table 1 Proximate and ultimate analyses of coal

Sample	Proximate analysis (wt%)				Ultimate analysis (wt%)			
	A	V	FC	C	H	N	S	O
LPS-R	15.62	38.90	45.48	62.81	4.57	1.11	3.28	28.23
LPS-D	2.46	42.09	55.45	73.28	5.22	1.00	3.79	16.71

3 Results and discussion

3.1 FTIR analysis

Figure 1 shows the infrared spectra of LPS-R and LPS-D by FTIR, from which it shows that the kaolin absorption peak located at 3700–3600 cm^{-1} (Fig. 1a) in LPS-R almost disappeared after acid treatment and the absorption peak intensity caused by minerals of 600–400 cm^{-1} (Fig. 1f) was notably reduced, indicating that acid treatment can remove a large number of ash such as clay and silicate in the coal. In addition, to distinguish the difference between LPS-R and LPS-D spectra, curve fitting method was adopted for analysis, and the spectrum was divided into four parts: aliphatic functional groups of 3000–2800cm^{-1} (Fig. 1b), oxygen-containing functional groups of 1750–1390 cm^{-1} (Fig. 1c) and 1390–960 cm^{-1} (Fig. 1d), and aromatic functional groups of 920–720 cm^{-1} (Fig. 1e). The curve-fitted results of the infrared spectra of LPS-R and LPS-D are shown in Fig. 2, where the correlation coefficient R^2 of each region are > 0.995. The functional group distribution and corresponding content of the two coals are shown in Table 2.

According to the relative contents of aliphatic structure fitting by peaks in Table 2, absorption peaks caused by CH_2 stretching vibration in LPS-R and LPS-D accounted for 80.34% and 78.85%, respectively, suggesting that the lipids in LPS-R and LPS-D were mainly in the form of long chains, with relatively few branched and side chains. After acid treatment, the proportion of symmetrical and asymmetric stretching vibration of $–CH_2$ in LPS-D decreased by 1.49%, indicating that the long aliphatic chain was destroyed and shortened slightly. The peak at around 1695 cm^{-1} was attributed to the stretching vibration of carboxylic acid, and the absorption strength increased by 13.04% after acid treatment, revealing that the alkali metal elements linked to COO– could be removed, forming COOH group. The peaks near 1600, 1565 and 1500 cm^{-1} were attributed to the conjugated extension vibration of aromatic C=C. The relative content of aromatic C=C reduced by 0.01% merely, indicating that the aromatic C = C skeleton was stable enough which was not damaged easily by acid treatment. At 1100–1350 cm^{-1}, the absorption vibration peaks were mainly caused by C–O and C–OH stretching vibration of ether oxygen and phenolic hydroxyl. The corresponding contents of hydroxyl increased from 22.28% to 55.93% and the contents of ether oxygen increased from 25.5% to 42.01%, due to the removal of a large number of alkali and alkaline earth metal associated with oxygen and hydroxyl groups by acid treatment. Additionally, the absorption peaks of silica-alumina minerals at 1010 and 1038 cm^{-1} almost disappeared after acid treatment. In LPS-R, benzene ring 3 substitution (accounting for 73.16%) was the dominant type of aromatic hydrocarbons, while benzene ring 4 substitution (accounting for 73.42%) was dominant in LPS-D after acid treatment, suggesting that the structure of aromatic hydrocarbons was altered by substitution reaction to a certain extent during acid treatment.

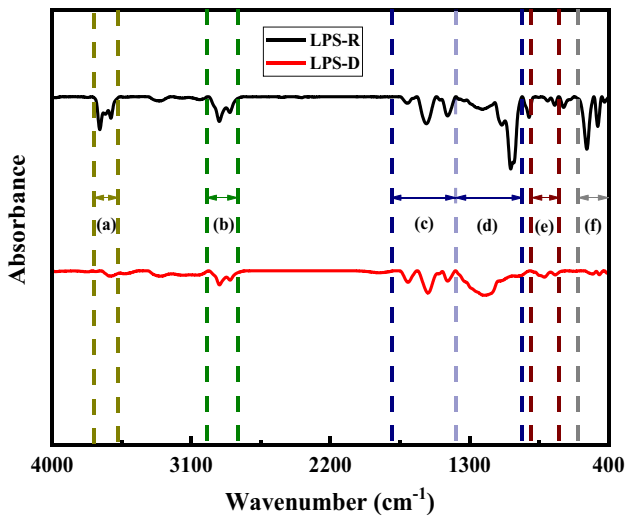

Fig. 1 FTIR spectra of LPS-R and LPS-D. **a** 3700–3600 cm^{-1} **b** 300–2800 cm^{-1} **c** 1750–1390 cm^{-1} **d** 1390–960 cm^{-1} **e** 920–720 cm^{-1} **f** 600–400 cm^{-1}

In order to better understand the chemical structure of LPS coal before and after acid treatment, the infrared structural parameters in Table 3 were analyzed to characterize the carbon skeleton structure of coal according to the intensity of fitting peaks. The aromatic carbon ratio f_a is calculated as follows:

$$f_a = 1 - \frac{C_{al}}{C} = 1 - \frac{H_{al}}{H} \times \frac{H}{C} \Big/ \frac{H_{al}}{C_{al}} \quad (1)$$

$$\frac{H_{al}}{H} = \frac{A_{3000-2800/cm}}{A_{920-720/cm} + A_{3000-2800/cm}} \quad (2)$$

In Eq. (1), C_{al}/C is the ratio of aliphatic carbon to total carbon, H_{al}/H is calculated by Eq. (2), which refers to the ratio of aliphatic hydrogen to total hydrogen content, H/C atomic ratio is calculated by ultimate analysis, and H_{al}/C_{al} takes the empirical value of 1.8.

Table 4 shows the infrared structural parameters of LPS-R and LPS-D referred in Table 3. The aliphatic hydrogen content I_1 of LPS-D decreased by 18.1%, while the structurally stable aromatic hydrogen content I_2 increased by 74% compared to that of LPS-R; The aliphatic hydrocarbon branch chain ratio (CH_3/CH_2) of LPS coal has little difference before and after demineralization, indicating that acid treatment has weak effect on the aliphatic side chain; *C'* and Doc increased by 62% and

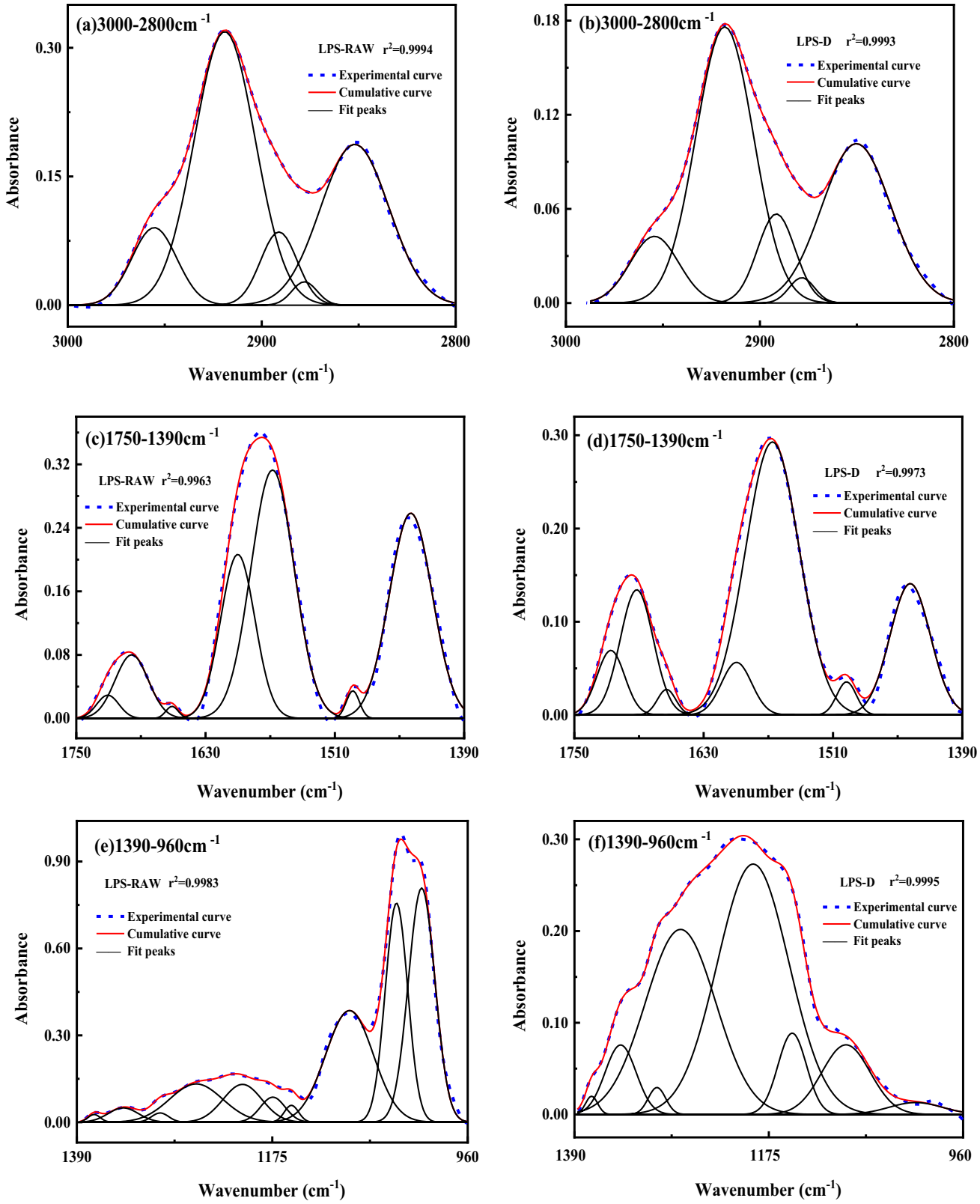

Fig. 2 Curve fittings of LPS-R and LPS-D sample's infrared spectrum in different wavenumber bands

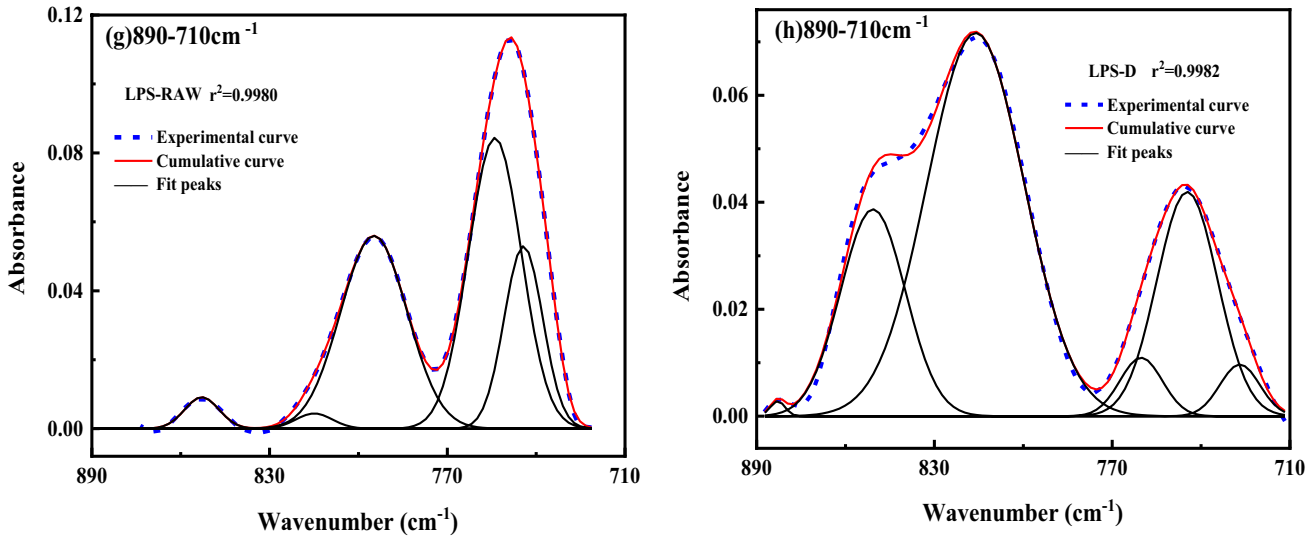

Fig. 2 (continued)

Table 2 Assignments for peaks in FTIR absorption wavenumber and corresponding content

Peak	Assignment	LPS-R		LPS-D	
		Center (cm^{-1})	Area (%)	Center (cm^{-1})	Area (%)
1	Asym.RCH_3	2955.4	10.14	2954.4	9.46
2	Asym.R_2CH_2	2919.0	48.41	2918.1	46.63
3	–R_3CH	2891.1	7.81	2891.5	9.90
4	Sym.RCH_3	2877.9	1.71	2878.4	1.89
5	Sym.R_2CH_2	2852.0	31.93	2850.3	32.22
6	Conjugated C=O	1720.8	1.83	1716.2	6.22
7	Carboxyl acids	1698.6	1.43	1692.1	14.47
8	Conjugated C=O	1661.1	0.53	1664.4	1.63
9	Aromatic C=C	1600.1	19.92	1599.5	5.56
10	Aromatic C=C	1567.9	38.04	1566.2	51.43
11	Aromatic C=C	1493.3	1.28	1497.4	2.24
12	Asym.CH_3–, CH_2–	1439.5	30.98	1438.4	18.45
13	CH_3-Ar, R	1371.0	0.44	1371.0	0.55
14	C–OH in phenols	1338.9	2.02	1338.9	5.38
15	C–O in cyclic ethers	1298.3	0.74	1298.7	1.17
16	C–O–C in cyclic ethers	–	–	1272.6	32.43
17	C–OH in phenols	1258.7	9.43	–	-
18	C–O in phenols	1207.8	6.82	–	–
19	C–OH in phenols	–	–	1192.3	44.76
20	C–O in phenols	1174.4	2.89	–	–
21	C–O in phenols	1153.9	1.12	1149.1	5.79
22	C–O in alcohols and ethers	1090.0	24.76	1089.5	8.41
23	Si–O	1038.3	22.88	–	–
24	Si–O	1010.7	28.90	1012.4	1.51
25	Five adjacent H deformation	–	–	882.9	0.32
26	Four adjacent H deformations	860–810	4.25	860–810	73.42
27	Three adjacent H deformations	810–750	73.16	810–750	3.60
28	Two adjacent H deformations	750–720	22.59	750–720	22.66

34% respectively, which suggests that the maturity of coal quality and the degree of aromatic ring polycondensation were promoted after acid treatment; The f_a increased by 11.5%, revealing that the aromatic structure increased; The oxygen enrichment degree (C=O/C–O) of LPS coal increased from 0.088 to 0.228, suggesting the C–O bond decreased and the C=O bond increased relatively; The A_{ar}/A_{al} of demineralized coal increased by 58%, revealing that acid washing treatment may lead to the formation of aromatic hydrocarbons, which were more stable. In general, the structural stability of LPS coal was enhanced to a certain extent after acid treatment on the basis of the infrared parameters.

3.2 ^{13}C-NMR analysis

Different carbon skeleton structures were investigated by solid state ^{13}C-NMR studies (Qian et al. 2014; Jing et al. 2019; Kawashima et al. 2000). According to the ^{13}C-NMR spectra of LPS-R and LPS-D in Fig. 3, both of them contain two main peak clusters, namely, which represent aliphatic carbon (0–90 ppm) and aromatic carbon (90–165 ppm). Meanwhile, they also contain a small amount of carbonyl carbon with chemical shift of 165–220 ppm. To clearly figure out the influence of demineralization on carbon skeleton structure, ^{13}C-NMR spectra were decoupled by peaks to analyze the structural parameters of LPS-R and LPS-D,

Table 3 Infrared structural parameters

Item	Parameter	Formula	Definition
Aliphatic structure	I_1	$A_{3000\text{-}2800/cm}/A_{1\text{-}28}$	The ratios of aliphatic hydrogen to all functional groups
	CH_3/CH_2	$A_{2955/cm}/A_{2920/cm}$	Length and branching degree of aliphatic chain in coal
Oxygen-containing functional group structure	C'	$A_{1800\text{-}1650/cm}/A_{1600/cm}+A_{1800\text{-}1650/cm}$	Maturity of coal
	C=O/C–O	$A_{1800\text{-}1650/cm}/A_{1260\text{–}1040/cm}$	The oxygen content of coal
Aromatic structure	I_2	$A_{900\text{–}700/cm}/A_{1\text{–}28}$	The ratios of aromatic hydrogen to all functional groups
	A_{ar}/A_{al}	$A_{1600\text{–}1500/cm}/A_{3000\text{-}2800/cm}$	The ratios of aromatic hydro- carbons to aliphatic hydrocarbons
	f_a	$1-C_{al}/C$	Aromatic carbon as a percentage of total carbon
	Doc	$A_{900\text{–}700\ /cm}/A_{1600/cm}$	Degree of condensation of aromatic rings

Table 4 Parameters of LPS-R and LPS-D samples calculated from FTIR spectra

Coal sample	I_1	CH_3/CH_2	C'	C=O/C–O	I_2	A_{ar}/A_{al}	f_a	Doc
LPS-R	0.149	0.147	0.330	0.088	0.027	0.944	0.590	0.576
LPS-D	0.122	0.144	0.535	0.228	0.047	1.493	0.658	0.772

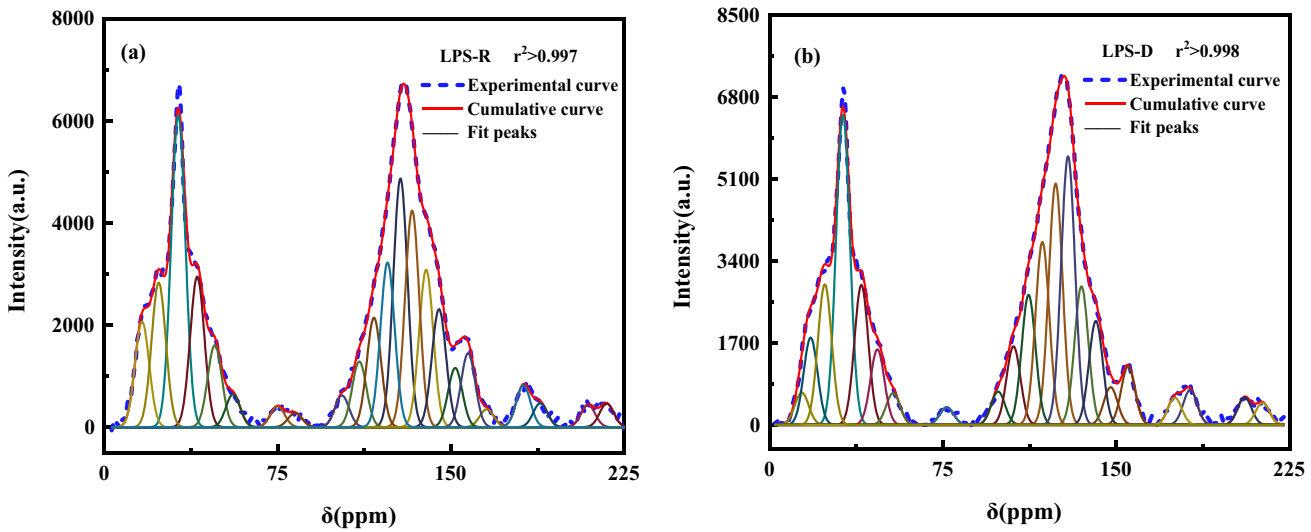

Fig. 3. ^{13}C-NMR spectra and the de-convoluted curves

which was shown in Table 5. LPS-R is mainly composed of aliphatic carbon and aromatic carbon, accounting for 38.72% and 55.84% respectively, the same as that of LPS-D, with the content of aliphatic carbon and aromatic carbon of LPS-D changed little by 1.18% and 1.47% respectively after acid treatment, suggesting that the macromolecular structure of LPS coal was not altered greatly. The total content of oxygen-containing functional group structures in LPS-R mainly consisted of oxy-aliphatic carbon $f_{al}^{O}=3.39\%$, oxy-aromatic carbon $f_a^{P}=5.76\%$, carboxyl and carbonyl carbon $f_a^{C}=6.72\%$, which decreased from 15.87% to 8.60% due to the protonation of oxygen-containing functional groups by acid treatment process. Based on the curve-fitted ^{13}C-NMR spectra results in Table 5, six lattice parameters were calculated and the results were summarized in Table 6. Seen from it, the average ratio of bridge carbon to peripheral carbon of aromatic compounds X_{BP}, which reflects the polycondensation degree of aromatic compounds, that is, the size of aromatic core, increased from 0.22 to 0.31 after acid treatment, indicating that demineralization process made the aromatic carbon condense to a greater extent, so as to increase the size of aromatic clusters. The number of C_a, C_{al}, C_{cl} and C_p increased by 45.6%, 37.6%, 41.9% and 27.4%, indicating that the LPS-D has larger cluster structures than LPS-R to a certain extent.

Table 6 Lattice parameters of LPS-R and LPS-D

Lattice parameters	Formula	LPS-R	LPS-D
X_{BP}	$X_{BP}=f_a^{B}/f_a'$	0.22	0.31
C_{cl}	$C_{cl}=C_a/f_a'\times0.01$	19.03	27.01
C_a	$C_a=3/(0.5—X_{BP})$	10.63	15.48
C_{al}	$C_{al}=C_{cl}\times f_{al}\times0.01$	7.37	10.14
C_p	$C_p=C_{cl}\times(f_a^{H}+f_a^{P}+f_a^{S})\times0.01$	8.31	10.59
R_a	$R_a=0.5\times(C_a—C_p)+1$	2.16	3.44

X_{BP}=ratio of bridge carbon to peripheral carbon; C_{cl}=total number of carbons per cluster; C_a=number of aromatic carbons per cluster; C_{al}=number of aliphatic carbons per cluster; C_p=number of peripheral carbons per cluster; R_a=aromatic rings

3.3 Thermogravimetric analysis.

Figure 4 shows the TG-DTG curves of LPS-R and LPS-D pyrolysis experiment by TG at three different heating rates. The characteristic temperature of coal pyrolysis are defined as follows: the initial pyrolysis temperature T_0 is defined at the intersection point of X axis and the line of sample conversion of 0.05 and 0.50 on the TG curve(Yan et al. 2019; Wang et al. 2016), and the peak temperature corresponding to $(dw/dt)_{max}$ is defined as T_p. The pyrolysis characteristic parameters of LPS-R and LPS-D are shown in Table 7. With the increase of heating rate, T_p of LPS-R coal shifted from 457.15 °C (20 °C/min) to 482.75 °C (60 °C/min), resulting in thermal hysteresis (Wang et al. 2022) in DTG curve. Based on Fig. 4 combined with Table 7, the TG curve decreases along with the increasing of temperature, and at 1000 °C, the mass weight loss of LPS-R or LPS-D at different heating rates are both close to the contents of their respective volatiles in Table 1 proximate analysis (LPS-RAW: 38.9%, LPS-D: 42.09%).

Taking the heating rate of 40 °C/min as an example, as can be seen from Table 7: the $(dw/dt)_{max}$ of LPS-R is 2.68%/min, and the $(dw/dt)_{max}$ of LPS-D is 2.54%/min. According to FTIR and ^{13}C-NMR analysis, the aliphatic hydrogen content I_1 and the content of aliphatic carbon of LPS-R are 0.149 and 38.72%, higher than that of LPS-D respectively. Therefore, the covalent bond breaking between aliphatic carbon in LPS-R can generate more small molecular tar fragments quickly at T_p, contributing to the result that the $(dw/dt)_{max}$ of LPS-R is 0.14%/min higher than that of LPS-D. The T_P of LPS-R and LPS-D are 471.89 °C and 473.79 °C

Table 5 Solid state^{13}C-NMR peak-fitting results of LPS-R and LPS-D

Chemical shift(ppm)	Structural fragments	Symbol	Relative area (%)	
			LPS-R	LPS-D
90–230	Aromatic carbon	f_a	61.28	62.46
90–165	Aromatic nucleus carbons	f_a'	55.84	57.31
165–230	Carbonyl and carboxyl carbon	f_a^{C}	6.72	5.16
100–129	Protonated aromatic carbons	f_a^{H}	24.57	30.44
129–165	Nonprotonated aromatic carbons	f_a^{N}	24.57	26.32
148–165	Oxy-aromatic carbon	f_a^{P}	5.76	2.60
137–148	Alkylated aromatic carbon	f_a^{S}	13.36	6.17
129–137	Aromatic bridgehead carbons	f_a^{B}	12.15	17.55
0–90	Aliphatic carbon	f_{al}	38.72	37.54
22–55	CH and CH_2	f_{al}^{H}	30.79	31.24
0–22	CH_3	f_{al}*	4.54	5.46
55–90	Oxy-aliphatic carbon	f_{al}^{O}	3.39	0.84

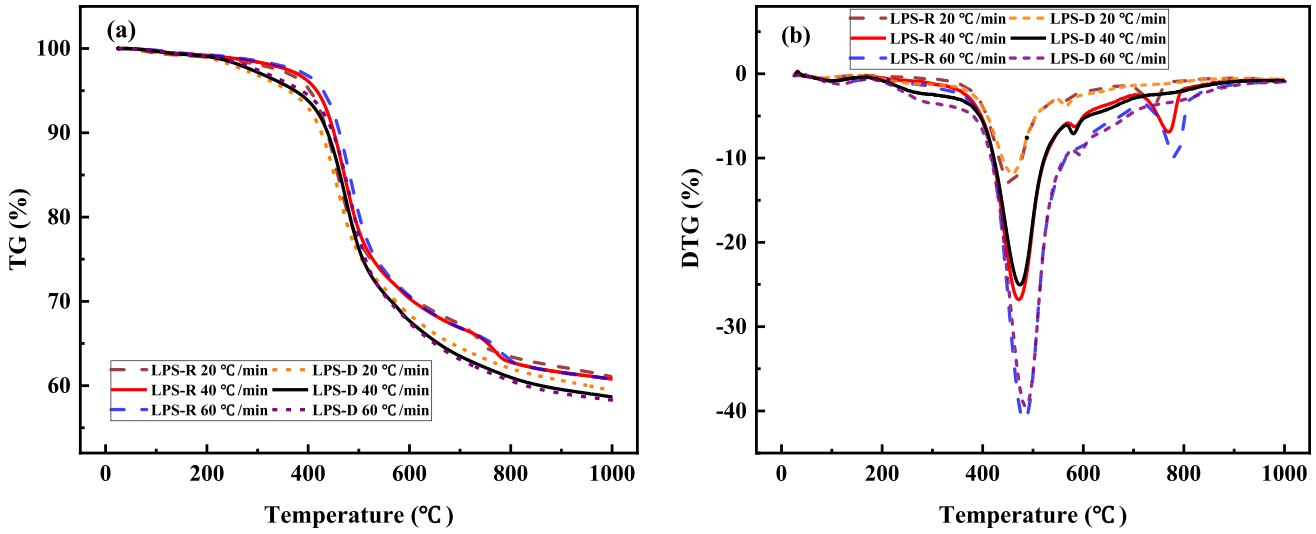

Fig. 4 Pyrolysis characteristic curve of LPS-R and LPS-D

Table 7 Pyrolysis characteristic parameters of LPS-R and LPS-D

Sample	Parameter	Heating rate (°C/min)		
		20	40	60
LPS-R	weight loss (%)	38.93	39.23	39.24
	$(dw/dt)_{max}$ (%/min)	1.31	2.68	4.11
	T_0 (°C)	273.18	301.20	316.91
	T_P (°C)	457.15	471.89	482.72
LPS-D	weight loss (%)	40.59	41.36	41.75
	$(dw/dt)_{max}$ (%/min)	1.18	2.54	3.95
	T_0 (°C)	215.61	234.44	247.01
	T_P (°C)	459.07	473.79	485.36

respectively. Compared with LPS-D, LPS-R contains more oxygen-containing functional groups (15.87%) with lower bond energy and less aromatic carbon (55.84%) with higher bond energy, which is easy to decompose, so the T_p is about 2 °C lower than that of LPS-D. Furthermore, as a pyrolysis reactivity parameter (Yan et al. 2020), T_p reflects the average stability of the macromolecular structure of coal (Han et al. 2013a, b), which indicates that LPS-R is more likely to fracture in the pyrolysis process, and the pyrolysis reactivity of LPS-R is higher.

As shown in Fig. 5, the pyrolysis process of LPS-R and LPS-D at the heating rate of 40 °C/min is divided into three stages according to the second derivative method (Wang et al.2016), among which the division of stage 1 and stage 2 is where the slope of TG curve changes obviously and the division of stage 2 and stage 3 is where the d^2m/dT^2 changed slightly. The first stage is related to water evaporation and gas desorption in coal pores, 25–222 °C for LPS-R and 25–205 °C for LPS-D. During this stage, the slope of TG curve drops little, and both DTG curve have a small water loss peak near 100 °C, contributed by the evaporation of crystal water in coal. The second stage is regarded as the main pyrolysis stage (LPS-R: 222–693 °C; LPS-D: 296–707 °C), TG curve slope gradually increases, DDTG curve is roughly sinusoidal, during this main pyrolysis stage, part of bridge bonds and side chains with weaker binding energy, oxygen-containing functional groups and macromolecular side chains undergo decomposition reaction successively making a great weight loss peak appeared in DTG curve. The third stage is related to the semi-coke condensation stage (LPS-R: 693–1000 °C; LPS-D: 707–1000 °C), in which pyrolytic coke is formed by polycondensation reaction. On the DTG curve of LPS-R at 780 °C, there is an obvious weight loss peak caused by the decomposition of minerals in ash such as carbonate (Cheng et al. 2019; Shi et al. 2013; Zhu et al. 2018), which almost disappeared on that of LPS-D after acid treatment.

The DTG curve is mainly caused by the cleavage of different covalent bonds in coal (Li et al. 2015). However, since pyrolysis is a process where overlapping reactions take place in series or in parallel, it is necessary to decouple the DTG curve to further intuitively analyze the effect of demineralization on pyrolysis behavior. To correlate the bond cleavage behavior with the coal pyrolysis, the generalized reduction gradient method (GRG) is used to resolve multiple subpeaks of DTG curve (Shi et al. 2013). The peak temperature of each subpeak is regarded as the average reaction temperature of chemical bond breaking, and the peak intensity is a measure of the corresponding mass loss. Figure 6 shows the curve-fitted DTG results and specific parameters are shown in Table 8.

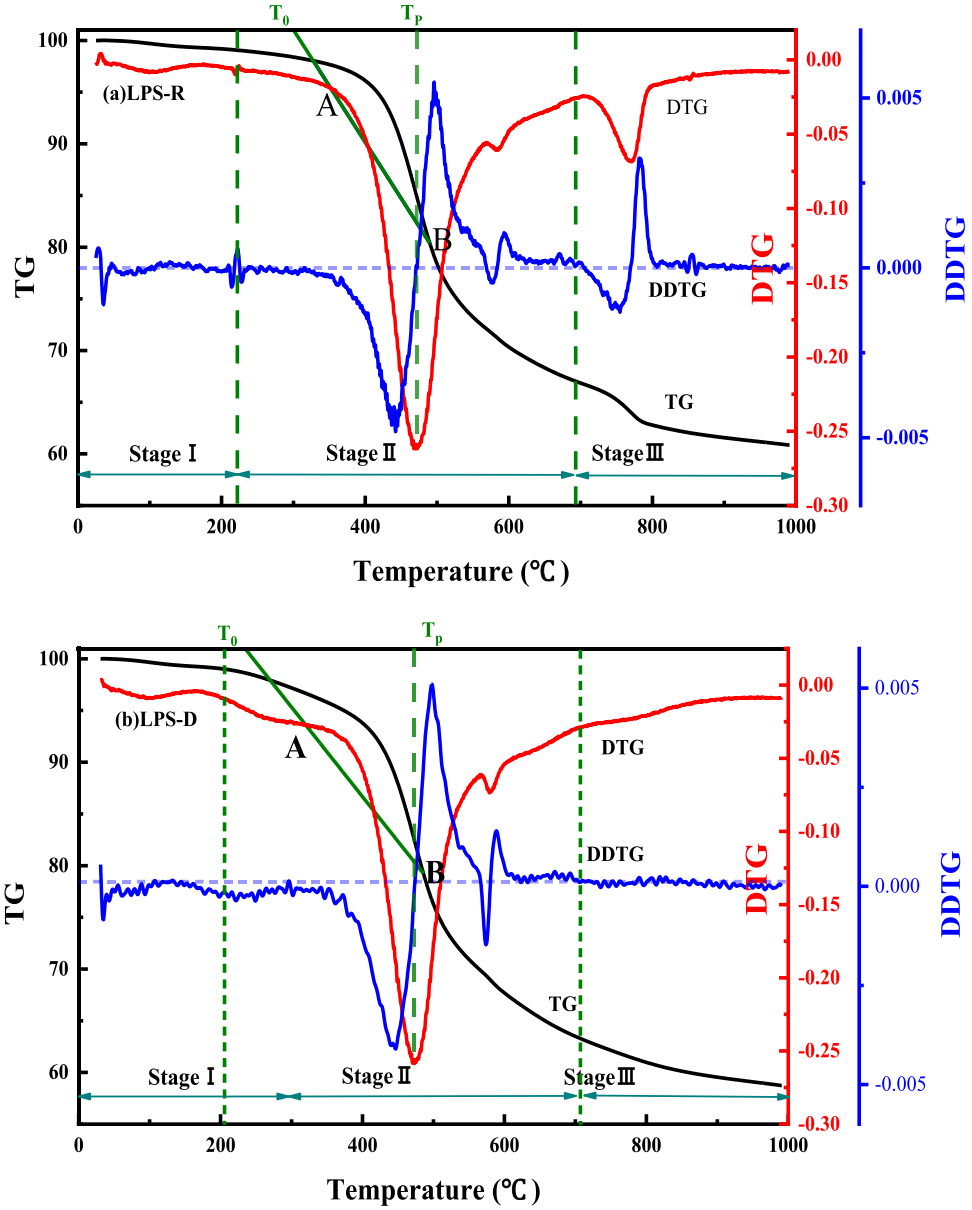

Fig. 5 TG, DTG and DDTG curves of LPS-R and LPS-D at heating rate of 40 °C/min

In Fig. 6, DTG curve of LPS-R and LPS-D were decoupled into six and five subpeaks according to GRG method (Shi et al. 2013) respectively, among which peak 1 was considered as the release of bound water and decomposition of carboxylic acid (Eskay et al. 1997), and a distinct weight loss peak appeared in DTG curve for both LPS-R and LPS-D at 250 °C. According to FTIR analysis, the proportion of carboxylic acid increased by 13.04% after acid treatment, thus the area of peak 1 for LPS-D was increased by 4.56% in Table 8. Peak 2 was related to the cleavage of covalent bonds formed by aliphatic carbon and heteroatoms on the side chain of aromatic structure, including Cal-O/N/S (Shi et al. 2013; Liu et al. 2008); peaks 3 and 4 were considered for the cleavage of chemical bonds centered on aliphatic carbon and aromatic carbon respectively, including Cal-O, Cal-Cal (Heek and Hodek 1994) and Car-O (Hodek et al. 1991); All peaks 2, 3 and 4 were the main organic devolatilization peaks, among which peak 3 for LPS-R and LPS-D occupied 65.43% and 65.59%, respectively, indicating that the cleavage of chemical bond in aliphatic carbon was the main cause for the weight loss of coal pyrolysis; Peak 5 was mainly caused by carbonate decomposition(Li et al. 2015), which was disappeared in LPS-D after acid treatment; Peak 6 was related to the polycondensation of aromatic rings (He et al. 2015). The evolution temperature of peak 6 for LPS-D was about 100 °C lower than that of LPS-R, and the area was 3.33% larger than that of LPS-R. This was mainly because acid treatment promoted the condensation of the aromatic structure, leading to the early release of volatiles, and similar conclusions were found in the study of Cheng et al (2019).

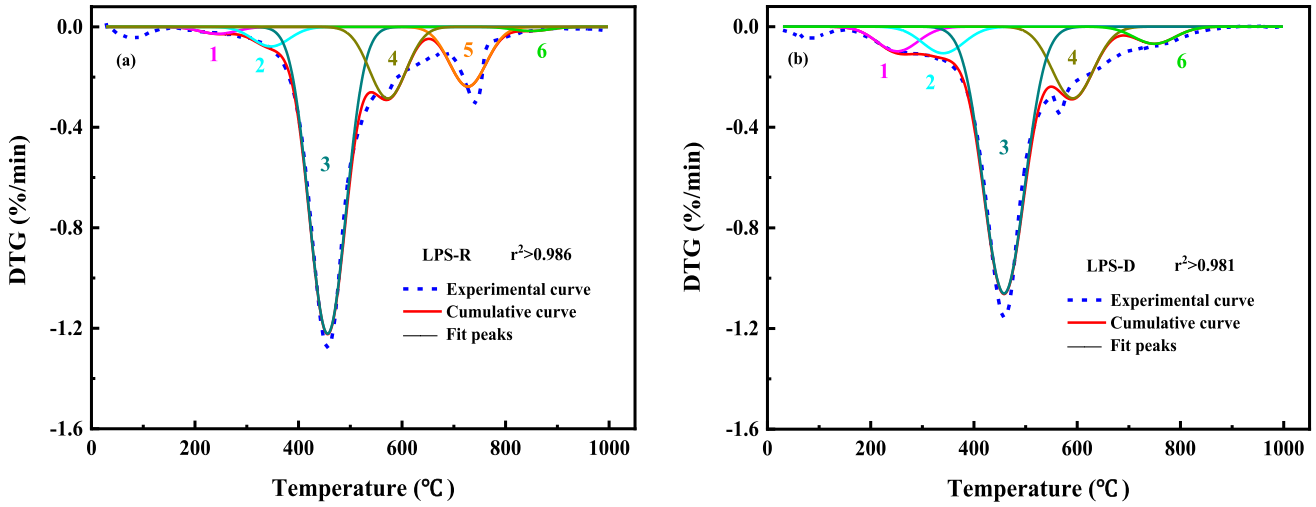

Fig. 6 DTG curve of LPS-R and LPS-D fitted by subcurves

Table 8 Fitting results of DTG curve

Peak		1	2	3	4	5	6
LPS-R	*T* (°C)	244.35	346.62	456.14	572.59	727.21	849.41
	Area (%)	1.49	4.19	65.43	15.26	12.75	0.88
LPS-D	*T* (°C)	251.62	340.34	458.30	591.55	–	749.75
	Area (%)	6.05	6.53	65.59	17.62	–	4.21

3.4 Kinetic analysis

The contents of various functional groups of LPS-R and LPS-D vary to some extent on the basis of the former analysis by FTIR and ^{13}C-NMR, and the reactivity of coal pyrolysis related to the thermal stability of functional groups can be reflected in the pyrolysis kinetics. According to the recommendations of Kinetics Committee of the International Confederation for Thermal Analysis and Calorimetry (Vyazovkin et al. 2011), as the crucial composition of coal pyrolysis, pyrolysis kinetics of iso-conversional method not only avoid the error brought by the mechanism function selection, making the calculated kinetic parameters more reliable, but also reveal the complex nature of the solid state reaction. Therefore, three iso-conversional methods, Starink (Khan et al. 2015), Flinn-Wall-Ozawa (FWO) (Flynn and Wall 1996; Ozawa 1965; Han et al. 2013a, b) and Distribution Activation Energy model (DAEM)(Miura and Maki 1998) were adopted in this study. The specific formulas are listed in Table 9 and the Arrhenius plots of the left side of the equations versus 1/*T* under different heating rates at specific conversion were presented in Fig. 7.

Figure 8 shows the pyrolysis conversion curves of LPS-R and LPS-D with temperature under different heating rates. It can be seen that when the temperature > 700 °C (corresponding to $\alpha \geq 0.7$), the coal pyrolysis is in the stage of semi-coke condensation. As the clusters of aromatic ring structure in coal char gradually become larger, the difficulty of polycondensation reaction also increases, so that the weight loss rate monotonically decreases, resulting in the curve of α-T gradually overlaps and finally shifts to low temperature with the increase of heating rate. At this stage, the linear correlation between $\ln(\beta/T^{1.92})$, $\ln\beta$, $\ln(\beta/T^2)$ and $1/T$ becomes poor due to the overlap of α-T curve, and the description of experimental data by kinetic fitting is likely to have a great deviation. Therefore, the specific parameters of apparent activation energy of LPS-R and LPS-D obtained by the three iso-conversional models at selected conversion from 0.05 to 0.65 are shown in Tables 10 and 11 and the apparent

Table 9 The isoconversional methods used in this study

Methods	Equation
Starink	$\ln\frac{\beta}{T^{1.92}} = -1.0008\frac{E}{RT} + \ln\frac{AR^{0.92}}{G(\alpha)E^{0.92}} - 0.312$
FWO	$\ln\beta = \ln\left(\frac{AR}{G(\alpha)E}\right) - 5.331 - 1.052\frac{E}{RT}$
DAEM	$\ln\frac{\beta}{T^2} = \ln\left(\frac{AR}{E}\right) + 0.6075 - \frac{E}{RT}$

Note: β, heating rate; A, pre-exponential factor; E, activation energy; R, universal gas constant (8.314 J/mol K); T, absolute temperature(K); $G(\alpha) = \int_0^T \frac{A}{\beta}\exp\frac{-E}{RT}dT$

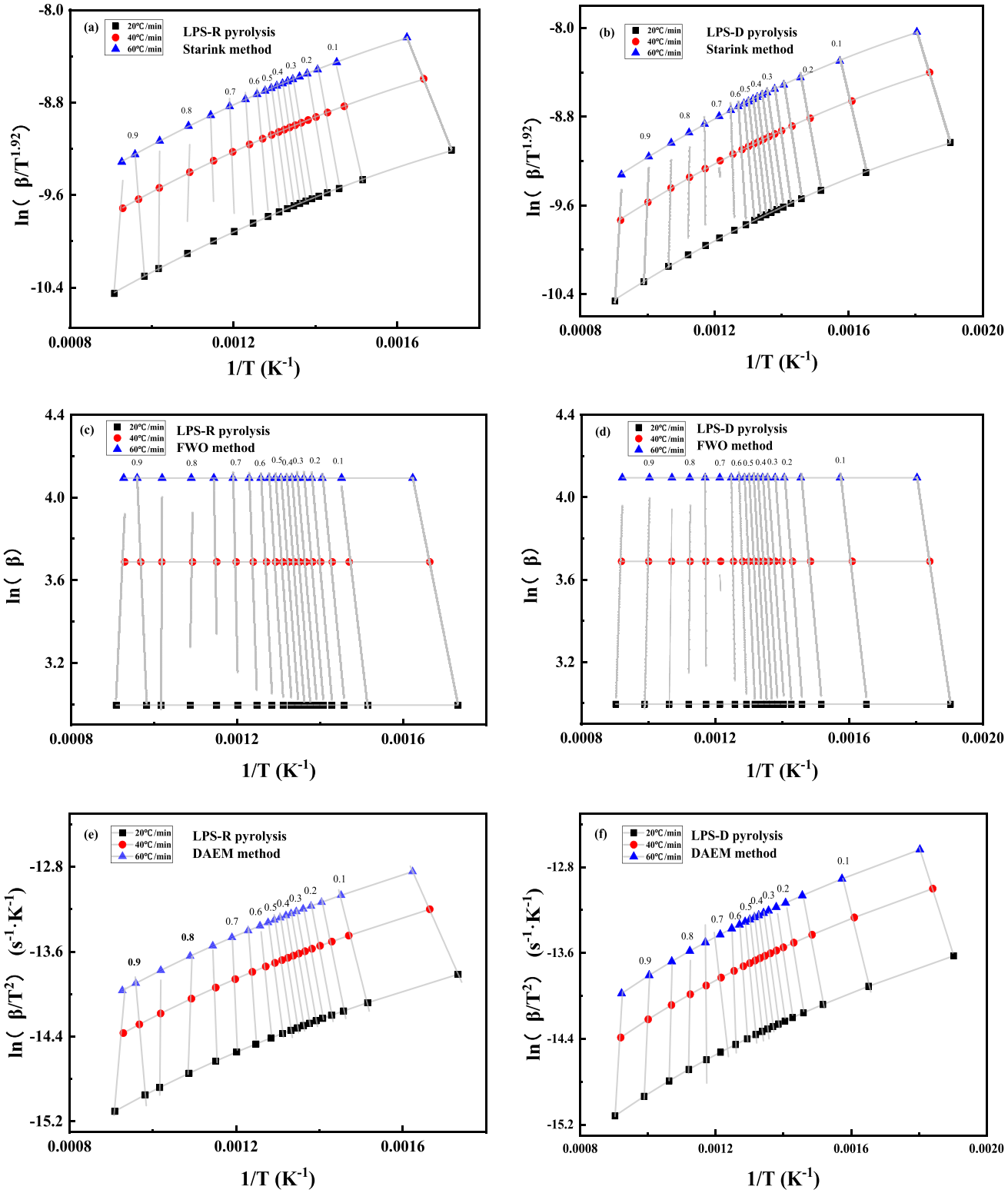

Fig. 7 Arrhenius plots of LPS-R and LPS-D with Starink, FWO and DAEM method

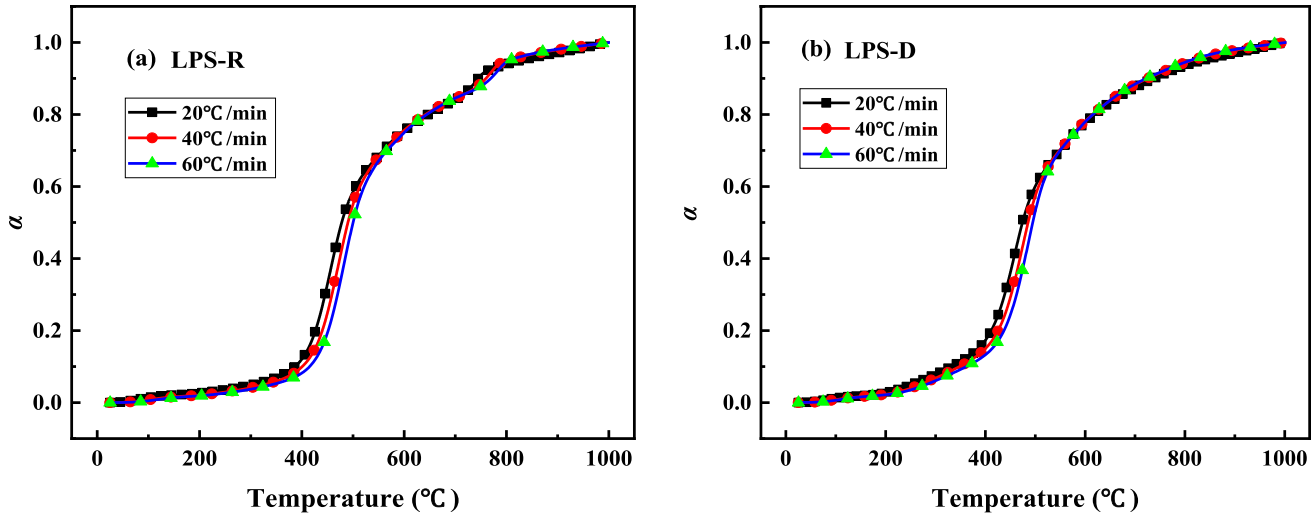

Fig. 8 Pyrolysis conversion curve of LPS-R and LPS-D with temperature at different heating rates

Table 10 Apparent activation energy of LPS-R pyrolysis determined by Starink, FWO and DAEM method

α	DAEM		FWO		Starink	
	E (kJ/mol)	R^2	E (kJ/mol)	R^2	E (kJ/mol)	R^2
0.05	73.66	0.99988	79.43	0.99992	74.00	0.99988
0.1	129.65	0.99116	133.89	0.99243	130.00	0.99121
0.15	161.81	0.98616	164.85	0.98800	162.14	0.98624
0.2	175.76	0.99179	178.33	0.99284	176.10	0.99184
0.25	183.65	0.99056	185.98	0.99172	183.98	0.99061
0.3	182.81	0.99057	185.32	0.99176	183.15	0.99063
0.35	194.76	0.99537	196.80	0.99594	195.10	0.99539
0.4	204.33	0.99575	206.01	0.99625	204.66	0.99577
0.45	208.10	0.99032	209.73	0.99142	208.44	0.99036
0.5	221.71	0.98499	222.80	0.98660	222.04	0.98506
0.55	253.71	0.98329	253.38	0.98488	254.02	0.98335
0.6	325.20	0.97068	321.57	0.97288	325.47	0.97077
0.65	468.96	0.95633	458.55	0.95865	469.12	0.95643
Average	214.16		215.13		214.48	

activation energy of LPS-R and LPS-D pyrolysis under different conversion is shown in Fig. 9.

As seen in Fig. 9, when $\alpha < 0.3$, since the aliphatic group of LPS-D contains more methyl carbon and methylene carbon, the chemical bonds with lower bond energy are easy to decompose at low temperature, the apparent activation energy of LPS-D is low, which indicates that acid treatment is conducive to promoting the pyrolysis reactivity of demineralized coal, resulting to the initial pyrolysis temperature T_0 of LPS-D lower than that of LPS-R (in Table 7, T_0 of LPS-D at different heating rates is 60–70 °C lower than that of LPS-R); When $0.3 \leq \alpha \leq 0.4$, the apparent activation energy of LPS coal before and after demineralization is the same; When $\alpha > 0.4$, it is in the main pyrolysis stage. The analysis of pyrolysis experiment shows that the stability of LPS coal increases after acid treatment, and a higher apparent activation energy is required for the cleavage of chemical bonds during LPS-D pyrolysis; When $\alpha = 0.65$, the activation energies of LPS-R and LPS-D increased significantly, indicating that stable structures such as aromatic bridgehead carbon (f_a^B) and protonated aromatic carbons (f_a^H) with high bond energy begin to destroy at high temperature. Since the content of f_a^B and f_a^H increased by 5.40% and 5.87% after acid treatment, the apparent activation energy of LPS-D is about 300 kJ/mol higher than that of LPS-R. The arithmetic mean activation energy values of LPS-R and LPS-D are 76 ± 4–463 ± 5 kJ/mol and 84 ± 2–758 ± 12 kJ/mol, respectively.

Table 11 Apparent activation energy of LPS-R pyrolysis determined by Starink, FWO and DAEM method

α	DAEM		FWO		Starink	
	E (kJ/mol)	R^2	E (kJ/mol)	R^2	E (kJ/mol)	R^2
0.05	82.55	0.99973	87.00	0.99980	82.85	0.99973
0.1	106.42	0.98556	110.96	0.98810	106.75	0.98568
0.15	138.76	0.98153	142.53	0.98425	139.10	0.98166
0.2	161.54	0.98585	164.58	0.98773	161.87	0.98593
0.25	177.86	0.99272	180.32	0.99365	178.19	0.99276
0.3	177.34	0.98120	180.02	0.98355	177.68	0.98130
0.35	195.15	0.98763	197.09	0.98908	195.48	0.98770
0.4	205.30	0.99146	206.88	0.99244	205.63	0.99150
0.45	222.42	0.99492	223.26	0.99548	222.74	0.99495
0.5	237.82	0.99075	238.05	0.99169	238.14	0.99079
0.55	279.84	0.99201	278.14	0.99271	280.13	0.99204
0.6	385.93	0.97599	379.18	0.97751	386.14	0.97605
0.65	771.68	0.91475	746.14	0.91738	771.59	0.91486
Average	241.74		241.09		242.02	

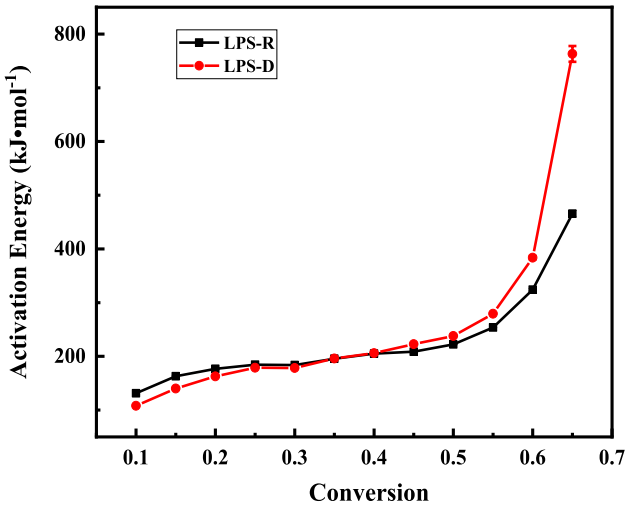

Fig. 9 Apparent activation energy of LPS-R and LPS-D pyrolysis at different conversion

4 Conclusions

The fundamental understanding of the pyrolysis characteristics of demineralized coal is considerable for the stable and efficient operation of the Oxy-Coal Combustion Steam System (OCCSS). In present study, the impact of acid treatment on pyrolysis characteristics of coal dependent on its chemical structure were investigated. FTIR and ^{13}C-NMR were used to characterize the chemical structure of LPS-R and LPS-D and the pyrolysis experiments were carried out by temperatures-programmed TG pyrolysis. The pyrolysis kinetics of LPS-R and LPS-D were analyzed by using three iso-conversional models. The main conclusions are as follows:

(1) FTIR shows that demineralization reduces the content of aliphatic hydrogen and C–O, increases the content of aromatic hydrogen and C=O, and improves the maturity of coal, making the chemical structure more stable.
(2) ^{13}C-NMR analysis shows that acid treatment has little effect on the proportion and distribution of aliphatic carbon and aromatic carbon, while LPS-D has a larger cluster structure and polycondensation degree of aromatic compounds due to the demineralization.
(3) TGA experiments indicate that the weight loss, which is mainly caused by the cleavage of aliphatic covalent bonds and the formation of small molecular fragments according to the curve-fitted DTG results, of LPS-D increased slightly by demineralization treatment, but the pyrolytic reaction at the $(dw/dt)_{max}$ decreased and the pyrolysis reactivity of LPS-R is higher.
(4) Kinetic analysis shows that acid treatment is conducive to promoting the pyrolysis reaction when $\alpha < 0.3$, whereas higher apparent activation energy is required for LPS-D in the semicoke polycondensation stages owing to the more stable chemical structure.

Acknowledgements LQ would like to acknowledge the financial support from the National Natural Science Foundation of China (51536002) and the Fundamental Research Funds for the Central Universities (2015QNA12). The financial contribution from the Open Sharing Fund for the Large-scale Instruments and Equipments of China University of Mining and Technology(CUMT) is also acknowledged.

Author contributions The manuscript was written through contributions of all authors. All authors have given approval to the final version of the manuscript.

Funding This work was supported by the National Natural Science Foundation of China (51536002), the Fundamental Research Funds for the Central Universities (2015QNA12) and the Open Sharing Fund for the Large-scale Instruments and Equipments of China University of Mining and Technology(CUMT).

Declarations

Competing interest The authors declare no competing financial interest.

References

Ahmed MA, Blesa MJ, Juan R, Vandenberghe RE (2003) Characterization of an Egyptian coal by Mossbauer and FTIR spectroscopy. Fuel 82:1825–1829

Cheng X, Shi L, Liu Q, Liu Z (2019) Effect of a HF-HF/HCl treatment of 26 coals on their composition and pyrolysis behavior. Energy Fuels 33:2008–2017

Cheng X, Shi L, Liu Q (2020) Heat effects of pyrolysis of 15 acid washed coals in a DSC/TGA-MS system. Fuel 268:117325

Cui Y, Li N, Fu Y, Chen L (2021) Carbon neutrality and mitigating contribution of terrestrial carbon sink on anthropogenic climate warming in China, the United States, Russia and Canada. J Geog Sci 31:925–937

Eskay TP, Britt PF, Buchanan AC (1997) Pyrolysis of aromatic carboxylic acids: potential involvement of anhydrides in retrograde reactions in low-rank coal. Energy Fuels 11:1278–1287

Flynn JH, Wall LA (1996) A quick direct method for determination of activation energy from thermogravimetric data. J Polym Sci Part C Polym Lett 4:323–328

Gómez-Serrano V, Fernández-González MC, Rojas-Cervantes ML, Alexandre-Franco MF, Macías-García A (2003) Carbonization and demineralization of coals: a study by means of FT-IR spectroscopy. Bull Mater Sci 26:721–732

Han F, Meng A, Lu W, Zhang Y, Li Q (2013a) Pyrolysis kinetics and product distribution of two coals. J Tsinghua Univ Sci Technol 53:348–352

Han Y, Li T, Saito K (2013b) A modified Ortega method to evaluate the activation energies of solid state reactions. J Therm Anal Calorim 112:683–687

He QQ, Wan KJ, Hoadley A, Yeasmin H, Miao ZY (2015) TG-GC-MS study of volatile products from Shengli lignite pyrolysis. Fuel 156:121–128

Heek KHV, Hodek W (1994) Structure and pyrolysis behaviour of different coals and relevant model substances. Fuel 73:886–896

Hodek W, Kirschstein J, Heek KHV (1991) Reactions of oxygen containing structures in coal pyrolysis. Fuel 70:424–428

Jing Z, Rodrigues S, Strounina E, Li M, Wood B, Underschultz JR, Esterled JS, Steel KM (2019) Use of FTIR, XPS, NMR to characterize oxidative effects of NaClO on coal molecular structures. Int J Coal Geol 201:1–13

Kawashima H, Yamashita Y, Saito I (2000) Studies on structural changes of coal density-separated components during pyrolysis by means of solid-state ^{13}C NMR spectra. J Anal Appl Pyrol 53:35–50

Khan AS, Man Z, Bustam MA, Kait CF, Ahmad P (2015) Impact of ball-milling pretreatment on pyrolysis behavior and kinetics of crystalline cellulose. Waste Biomass Valorization 7:571–581

Leng H, Feng D, Gao J, Zhang Y, Zhao Y-J, Du Q, Chang G-Z, Guo Q-J, Wang X, Sun S-Z (2021) Effect of high-temperature and microwave expanding modification on reactivity of coal char for char-NO interaction. Sci Total Environ 760:144028

Li ZK, Wei X-Y, Yan H-L, Zong Z-M (2015) Insight into the structural features of Zhaotong lignite using multiple techniques. Fuel 153:176–182

Li W, Bai Z, Bai J, Li X (2017) Transformation and roles of inherent mineral matter in direct coal liquefaction: a mini-review. Fuel 197:209–216

Li X, Li H, Wang R, Feng J, Li W (2019) Acid pretreatment effect on oxygen migration during lignite pyrolysis. Fuel 262:116650

Lin D, Qiu P, Xie X, Zhao Y, Chen G, Zeng L (2017) Chemical structure and pyrolysis characteristics of demineralized Zhundong Coal. Energy Sour Part A Recovery Util Environ Effects 40:282–287

Liu Q, Hu H, Zhou Q, Zhu S, Chen G (2004) Effect of inorganic matter on reactivity and kinetics of coal pyrolysis. Fuel 83:713–718

Liu Q, Wang S, Zheng Y, Luo Z, Cen K (2008) Mechanism study of wood lignin pyrolysis by using TG-FTIR analysis. J Anal Appl Pyrol 82:170–177

Liu J, Ma J, Luo L, Zhang H, Jiang X (2017a) Pyrolysis of superfine pulverized coal. Part 5. Thermogravimetric analysis. Energy Convers Manag 154:491–502

Liu L, Kumar S, Wang Z, He Y, Cen K (2017b) Catalytic effect of metal chlorides on coal pyrolysis and gasification part I. Combined TG-FTIR study for coal pyrolysis. Thermochim Acta 655:331–336

Liu F, Zhao J, Xuan G, Zhang F, Yang L (2021) Spatial evolution characteristics of active components of copper-iron based oxygen carrier in chemical looping combustion. Fuel 306:121650

Mandapati RN, Ghodke PK (2021) Kinetic modeling of Indian lignites pyrolysis in the context of underground coal gasification (UCG). Fuel 283:118939

Miura K, Maki T (1998) A simple method for estimating, f(E) and ko(E) in the distributed activation energy model. Energy Fuels 12:864–869

Ozawa T (1965) A new method of analyzing thermogravimetric data. Bull Chem Soc Jpn 38:1881–1886

Qian L, Zhao Y, Sun S, Che H, Chen H, Wang D (2014) Chemical/physical properties of char during devolatilization in inert and reducing conditions. Fuel Process Technol 118:327–334

Qiu PY, Zhao X, Chen J, Xu Y, Du LF, Sun S (2014) Effects of alkali and alkaline earth metals on pyrolysis characteristics and kinetics of Zhundong coal. J Fuel Chem Technol 42:1178–1189

Shi L, Liu Q, Guo X, Wu W, Liu Z-Y (2013) Pyrolysis behavior and bonding information of coal—a TGA study. Fuel Process Technol 108:125–132

Slyusarskiy KV, Larionov KB, Osipov VI, Yankovsky SA, Gubin VE, Gromov AA (2017) Non-isothermal kinetic study of bituminous coal and lignite conversion in air and in argon/air mixtures. Fuel 191:383–392

Song Y, Feng W, Li N, Li Y, Zhi K, Teng Y, He R, Zhou H, Liu Q (2016) Effects of demineralization on the structure and combustion properties of Shengli lignite. Fuel 183:659–667

Song Q, Zhao H, Jia J, Yang L, Lv W, Gu Q, Shu X (2020) Effects of demineralization on the surface morphology, microcrystalline and thermal transformation characteristics of coal. J Anal Appl Pyrol 145:104716

Sonibare OO, Haeger T, Foley SF (2010) Structural characterization of Nigerian coals by X-ray diffraction, Raman and FTIR spectroscopy. Energy 35:5347–5353

Sun S, Meng S, Xu H, Qiu P, Sun R, Zhao YJ, Guo YZ, Qiu PH, Qin Y (2012) A coal based Fuel near zero emission power generation system and method. China Patent, CN102628401A, filed April 24, 2012, and issued August 8, 2012

Vyazovkin S, Burnham AK, Criado JM, Pérez-Maqueda LA, Popescu C, Sbirrazzuoli N (2011) ICTAC kinetics committee recommendations for performing kinetic computations on thermal analysis data. Thermochim Acta 520:1–19

Wang J, Li P, Liang L, Yang J, Hao X, Guan G, Huang W (2016) Kinetics modeling of low-rank coal pyrolysis based on a three-gaussian distributed activation energy model (DAEM) reaction model. Energy Fuels 30:9693–9702

Wang Z, Xu M, Fu X, Cao J, Li C, Feng M, Li K (2022) Study on pyrolysis characteristics and kinetics of bituminous coal by thermogravimetric method. Combust Sci Technol 194:558–573

Yan J, Jiao H, Li Z, Lei Z, Wang Z, Ren S, Shui H, Kang S, Yan H, Pan C (2019) Kinetic analysis and modeling of coal pyrolysis with model-free methods. Fuel 241:382–391

Yan J, Liu M, Feng Z, Bai Z, Yan H (2020) Study on the pyrolysis kinetics of low-medium rank coals with distributed activation energy model. Fuel 261:116539

Yang Z, Duan L, Li L, Anthony EJ (2021) Movement and combustion characteristics of densified rice hull pellets in a fluidized bed combustor at elevated pressures. Fuel 294:120421

Zhang W, Sun S, Zhu H, Zhang L, Zhao Y, Wang P (2021) The evolution characteristics of bituminous coal in the process of pyrolysis at elevated pressure. Fuel 302:120832

Zhao Y, Zhang W, Wang P, Liu P, Zeng G, Sun S, Zhang S (2018) Kinetic characteristics of in-situ char-steam gasification following pyrolysis of a demineralized coal. Int J Hydrog Energy 43:10991–11001

Zhu P, Luo A-Q, Zhang F, Lei Z-P, Zhang J-L, Zhang J-S (2018) Effects of extractable compounds on the structure and pyrolysis behaviours of two Xinjiang coal. J Anal Appl Pyrol 133:128–135

Zhu P, Quan S, Lei Z, Zhang J (2019) Structural and pyrolysis behaviors analysis of coal pretreated with a weak acid. Energy Sour Part A Recovery Util Environ Effects 43:660–671